Generalized Equalization Enhanced Phase Noise in Coherent Optical Transceivers Using Arbitrary Raised Cosine Filters

Liu, Yuheng; Yi, Xingwen; Zhang, Jing; Lu, Guo-Wei; Li, Fan

Journal of Lightwave Technology

DOI:
10.1109/JLT.2024.3454977

E-pub ahead of print: 05/09/2024

Peer reviewed version

Generalized Equalization-Enhanced Phase Noise in Coherent Optical Transceivers Using Arbitrary Raised Cosine Filters

Yuheng Liu, Xingwen Yi, Jing Zhang, Guo-Wei Lu, and Fan Li

***Abstract*— Equalization-enhanced phase noise (EEPN) can degrade the performance of high baud-rate and long-distance coherent optical transmission systems that use electronic dispersion compensation (EDC). Existing theoretical calculations of EEPN are based on the ideal Nyquist filter, which has an unrealizable brickwall response due to its infinite time-domain extent. In this paper, we generalize the EEPN calculation for coherent optical transceivers using arbitrary raised cosine (RC) filters. We demonstrate that when the roll-off factor changes from zero to non-zero, the unitary transmission channel assumption no longer holds in the presence of EEPN. We calculate the resulting energy loss for transceivers using RC filters with arbitrary roll-off factors. The results indicate that while the intra-symbol EEPN remains almost unchanged, the inter-symbol EEPN and the total EEPN decrease with increasing bandwidth. Furthermore, we extend our analysis to high-order modulation formats, where the EEPN distribution varies depending on the moduli of the constellation clusters.**

***Index Terms*—Optical fiber communication, equalization enhanced phase noise, raised cosine filter, phase noise, quadrature amplitude modulation.**

I. Introduction

High baud rate transmissions have always been pursued in optical fiber communications to achieve cost-effective high-capacity transmission, with the state of the art exceeding 190 GBaud or 1 Tb/s per channel with high-order modulation formats [1][2][3][4][5]. They are combined with digital coherent detection and dispersion compensation to support long-distance transmissions over dispersive fiber. In such systems, Shieh *et al.* identified equalization-enhanced phase noise (EEPN) and conducted a theoretical analysis [6]. EEPN was shown to be proportional to the baud rate, length of fiber, and laser linewidth. Consequently, EEPN becomes more pronounced in high baud-rate and long-haul coherent optical transmissions [7][8][9]. EEPN has been further studied in the context of timing jitter, its interaction with nonlinear compensation, and mode-division multiplexing transmissions [10][11][12]. In [13], we have showed that the intra-symbol EEPN scales with the power of the individual constellation points/clusters, while the inter-symbol EEPN scales with the average power of the whole constellation. Therefore, for higher-order constellations with multiple moduli, the total EEPN, as well as the EEPN-induced phase noise and amplitude noise, distribute differently depending on the moduli.

However, existing studies on EEPN have primarily focused on ideal Nyquist filters with brickwall frequency responses, which are not realizable due to their infinite time-domain extent. Recently, we have studied the characteristics of EEPN with raised-cosine (RC) filters using different roll-off factors [14], and observed some interesting characteristics of EEPN. However, that report did not provide a theoretical analysis.

In this paper, we perform a rigorous study on the observations in [14]. We generalize the EEPN calculation for coherent optical transceivers with arbitrary raised-cosine (RC) filters. We find that the transmission channel becomes non-unitary when the roll-off factor is larger than zero. Subsequently, we calculate the resulted energy loss and revise the theoretical results of EEPN. Furthermore, we update our discussion about the EEPN distribution across constellation clusters with different moduli. All closed-form expressions are verified by the corresponding simulation results.

This paper is organized as follows. In Section II, we derive the energy loss from the non-unitary channel affected by EEPN and update the results for intra-symbol and inter-symbol EEPN. In Section III, we extend the results from Section II to high-order modulation formats, discussing the moduli-dependent EEPN distributions.

Manuscript received xxx; revised xxx; accepted xxx. Date of publication xxx; date of current version xxx. This work was supported in part by the National Key R&D Program of China (2022YFB2903004), National Natural Science Foundation of China (62271517, 62331013), JSPS KAKENHI grant (23K22760), Guangdong Basic and Applied Basic Research Foundation (2023B1515020003), State Key Laboratory of Advanced Optical Communication Systems and Networks of China (2024GZKF19), North Wales Growth Deal through Ambition North Wales, the UK GOV DSIT (FONRC) project REASON, the Engineering and Physical Sciences Research Council Project TITAN (EP/Y037243/1), and the International Science and Technology Cooperation Program of Sichuan Province (2023YFH0067). (*Corresponding author: Xingwen Yi.*)

Yuheng Liu and Fan Li are with the School of Electronics and Information Technology, Guangdong Provincial Key Laboratory of Opto-Electronic Information Processing Chips and Systems, Sun Yat-Sen University, Guangzhou 510275, China (e-mail: liuyh369@mail2.sysu.edu.cn; lifan39@mail.sysu.edu.cn).

Xingwen Yi is with the School of Computer Science and Engineering, Bangor University, LL57 1UT, UK (e-mail: x.yi@bangor.ac.uk).

Jing Zhang is with the Key Laboratory of Optical Fiber Sensing and Communications University of Electronic Science and Technology of China, Chengdu, Sichuan 610000, China (e-mail: zhangjing1983@uestc.edu.cn).

Guo-Wei Lu is with the Institute for Materials Chemistry and Engineering, Kyushu University, 6-1 Kasuga-koen, Kasuga, Fukuoka 816-8580, Japan (e-mail: gordon.guoweilu@gmail.com).

Color versions of one or more of the figures in this article are available online at http://ieeexplore.ieee.org

II. GENERALIZED EEPN

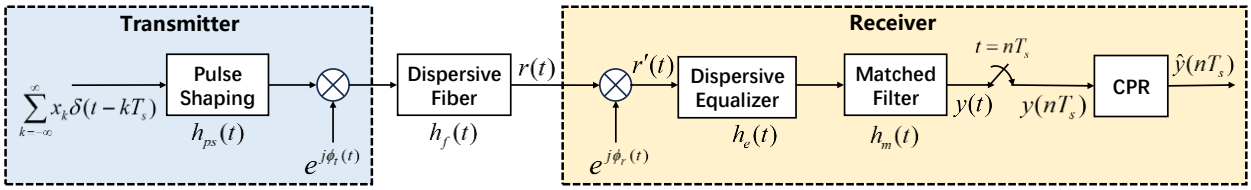

Fig. 1. General model of digital coherent optical systems using digital dispersion compensation.

Our analysis and terminology follow those in [6][7]. For clarity, we illustrate a general model of a digital coherent optical system with electronic dispersion compensation (EDC) in Fig. 1. The transmitted symbols x_k are assumed to be independent and identically distributed, with T_s representing the symbol period. The symbol train passes through pulse shaping with a root raised cosine (RRC) filter $h_{ps}(t)$ to generate a bandwidth-limited signal. The transmitter introduces a phase noise $e^{j\phi_t(t)}$ by the transmitter laser. We will ignore it in this paper because the transmitter phase noise has no effect on EEPN [6] when the fiber dispersion compensation is conducted at the receiver. For optical fibers, we only include the chromatic dispersion effect.

At the coherent receiver side, the local oscillator (LO) also introduces phase noise $e^{j\phi_r(t)}$. The electrical dispersion equalizer $h_e(t)$ compensates for the fiber dispersion $h_f(t)$. The matched filter $h_m(t)$ is matched to the pulse shaping filter at the transmitter, and their convolution results in an RC filter, as given in the Appendix, with a roll-off factor β ranging from 0 to 1. After down-sampling to symbol intervals, the signal undergoes carrier phase recovery (CPR) to obtain the estimated signal.

From Fig. 1, the output of the matched filter in the time domain can be written as

$$y(t) = r'(t) \otimes h_e(t) \otimes h_m(t)\,, \tag{1}$$

where

$$r'(t) = \left[\sum_{k=-\infty}^{\infty} x_k \delta(t - kT_s)\right] \otimes h_{ps}(t) \otimes h_f(t) \times e^{j\phi_r(t)}. \tag{2}$$

As discussed in [6], the phase noise and pulse shaping can be commuted due to the relatively short duration of the pulse shaping function. The convolution of the pulse shaping filter and the matched filter is an RC filter, given by

$$h_{rc}(t) = h_{ps}(t) \otimes h_m(t)\,. \tag{3}$$

Therefore, the output signal after the matched filter is

$$\begin{aligned} y(t) = &\left[\sum_{k=-\infty}^{\infty} x_k \delta(t - kT_s)\right] \\ &\otimes h_{rc}(t) \otimes h_f(t) \times e^{j\phi_r(t)} \otimes h_e(t) \end{aligned}, \tag{4}$$

where x_k represents the transmitted k^{th} information symbol, and $y(t)$ is sampled at the symbol rate $1/T_s$,which gives the digital sequence $y(nT_s)$. In this section, the CPR assumes ideal knowledge of the LO phase noise, and the estimated transmitted symbol is

$$\hat{y}(nT_s) = y(nT_s) e^{-j\phi(nT_s)}\,. \tag{5}$$

We convert the convolution in Eq. (4) to the frequency domain and arrive at

$$\begin{aligned} y(t) = &\sum_{k=-\infty}^{\infty} x_k \int_{-\infty}^{\infty} X_{LO}(f) \\ &\cdot h_1\left(t - kT_s - \frac{rf}{\pi}\right) \cdot e^{-jrf^2} \cdot e^{j2\pi ft} df \end{aligned}, \tag{6}$$

where $X_{LO}(f)$ is the Fourier transform of $e^{j\phi_r(t)}$, r is a dispersion related parameter defined in Appendix.

The second order moment of the signal is,

$$E[|y(t)|^2] = \sum_{k=-\infty}^{\infty} E[|x_k|^2] \cdot \int_{-\infty}^{\infty} \left| h_{rc}\left(t - kT_s - \frac{rf}{\pi}\right)\right|^2 S(f) df \tag{7}$$

where $E[\square]$ stands for the average operation and $S(f)$ is the spectral density of $e^{j\phi_r(t)}$, which follows a Lorentzian line shape.

Following a similar calculation in [6], we transmit an isolated "1" symbol, i.e., $x_k = 1$ for k=0, otherwise 0. Note that this condition is used in all the ensuing derivations in this section. Then the received signal is down sampled at one sample per symbol. Eq. (7) is subsequently simplified as

$$E[|y_1(nT_s)|^2] = \int_{-\infty}^{\infty} \left| h_{rc}\left(nT_s - \frac{rf}{\pi}\right)\right|^2 \cdot S(f) df\,, \tag{8}$$

where we use y_1 to emphasize that an isolated "1" symbol is transmitted. Then, the received total energy of the signal, sampled at the symbol interval, is

$$\begin{aligned} E_{1,\text{total}} &= \sum_{n=-\infty}^{\infty} E[|y_1(nT_s)|^2] \\ &= \sum_{n=-\infty}^{\infty} \int_{-\infty}^{\infty} \left| h_{rc}\left(nT_s - \frac{rf}{\pi}\right)\right|^2 \cdot S(f) df \end{aligned}. \tag{9}$$

Note that this total energy $E_{1,\text{total}}$ is assumed to be unity in [6] due to the unitary channel assumption. However, this needs to be revisited for arbitrary raised-cosine (RC) filters, specifically when the roll-off factor is non-zero.

A. Energy loss of the arbitrary RC filter in the presence of EEPN

The calculation process of the total energy in Eq. (9) is provided in Appendix, and with a slight approximation, the result is simplified as,

$$E_{1,\text{total}} = 1 - \frac{\beta}{2}\alpha\,, \tag{10}$$

where $\alpha = \pi^2 \cdot \beta_2 \cdot l \cdot f_{3dB} / T_s$, and f_{3dB} is the 3dB-linewidth

of the LO laser. Apparently, for the brickwall Nyquist filter with $\beta = 0$, the total energy is 1. This verifies the assumption in [6] that the transmission channel is unitary when $\beta = 0$. However, the transmission channel is not unitary when $\beta > 0$, and the loss can be deduced from Eq. (10).

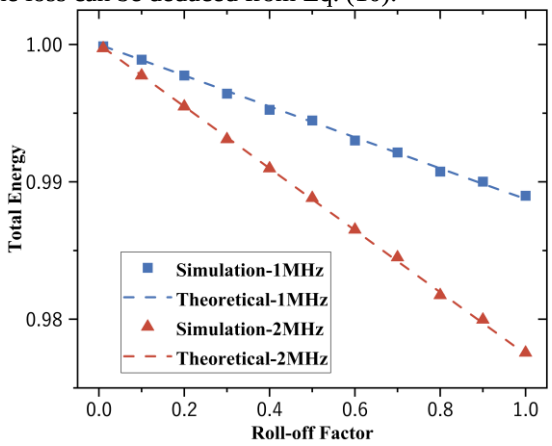

Fig. 2. Total energy for different laser linewidths and roll-off factors when an isolated "1" symbol is transmitted. The theoretical results (dashed lines) are calculated using Eq. (10).

We conducted a simulation of Fig. 1 to verify Eq. (10). The key simulation parameters are as follows: the fiber length is 2000 km, the dispersion coefficient is 16 ps/nm/km, and the symbol rate is 56 GBaud. Fig. 2 shows that the total energy decreases as the roll-off factor increases. The simulation results are overlaid with the theoretical calculation, confirming the accuracy of our calculation.

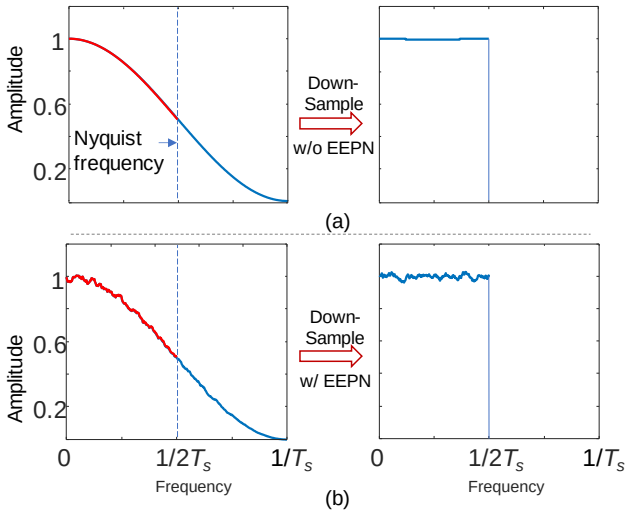

Fig. 3. Frequency response demonstrating the effects of EEPN after down-sampling. (a) Ideal RC filter without EEPN. (b) Distorted RC filter with EEPN, showing a roll-off factor of 1. Only positive frequencies are plotted for simplicity.

This phenomenon can be explained by EEPN-induced timing jitter [10]. During down-sampling, optimal sampling points loses energy. This can also be understood in the frequency domain. Figure 3 illustrates the simulated channel response for a roll-off factor of 1, with and without EEPN. Without EEPN, the channel response resembles the ideal RC filter, satisfying the Nyquist inter-symbol-interference (ISI) criterion with zero ISI. Frequencies above the Nyquist frequency perfectly fold back and sum up to a constant, resulting in no energy loss. However, with EEPN, the channel's frequency response exhibits random ripples. As a result, the expected odd symmetry around the Nyquist frequency is disrupted, and the folded channel response cannot consistently sum to a constant after down-sampling. Consequently, the leakage of some spectral components leads to energy loss, and the rippling frequency response manifests as ISI.

For simplicity, Fig. 3 does not illustrate the results when $\beta = 0$, because it is apparent that the frequency response is already limited within Nyquist frequency, and no spectrum leakage or energy loss will occur after down-sampling.

B. Generalized EEPN

Following the description in [6], we can first calculate the intra-symbol EEPN, total EEPN, and then deduce the inter-symbol EEPN.

The exact result of intra-symbol generalized EEPN is given in Appendix, and with a slight approximation, the intra-symbol EEPN is

$$EEPN_{\text{intra}} = D[y_1(0)] \approx \frac{1}{3}\alpha . \tag{11}$$

The total EEPN is deduced from the energy loss in the received symbol energy, which can be calculated using Eqs. (A8) and (A11) as

$$\left|E[y_1(0)]\right|^2 \approx 1-(1+c\beta^2)\alpha , \tag{12}$$

where $c = 1+\frac{4}{\pi^2}\cdot(-2+\cos(\frac{1-\beta}{2\beta}\pi)+\cos(\frac{1+\beta}{2\beta}\pi))$, a variable depending on β.

Therefore, with the help of Eq. (10), the total EEPN can be calculated as

$$EEPN = E_{1,\text{total}} - \left|E[y_1(0)]\right|^2 \approx (1-\frac{1}{2}\beta+c\beta^2)\alpha . \tag{13}$$

Note that we have substituted the energy loss of the transmission channel from Eq. (13) instead of assuming unity.

Finally, the inter-symbol EEPN is deduced as

$$EEPN_{\text{inter}} = EEPN - EEPN_{\text{intra}} \approx (\frac{2}{3}-\frac{1}{2}\beta+c\beta^2)\alpha . \tag{14}$$

We simulate an ideal QPSK transmission to verify the aforementioned results. The simulation parameters are the same as those in the subsection A. Fig. 4 shows the variations of total EEPN and intra-symbol EEPN for different roll-off factors with 100 kHz and 1 MHz laser linewidths, respectively. The intra-symbol EEPN shows little change. This is consistent with the approximation result in Eq. (11), which is independent of the roll-off factor. However, the total EEPN decreases as the roll-off factor increases. This is one of the major contributions of this paper, as it is somewhat counterintuitive: one might expect that a larger bandwidth would lead to a stronger interaction between the local oscillator phase noise and dispersion

equalization.

The inset constellation for a larger roll-off factor becomes more elliptical, which will be further explained in the next section.

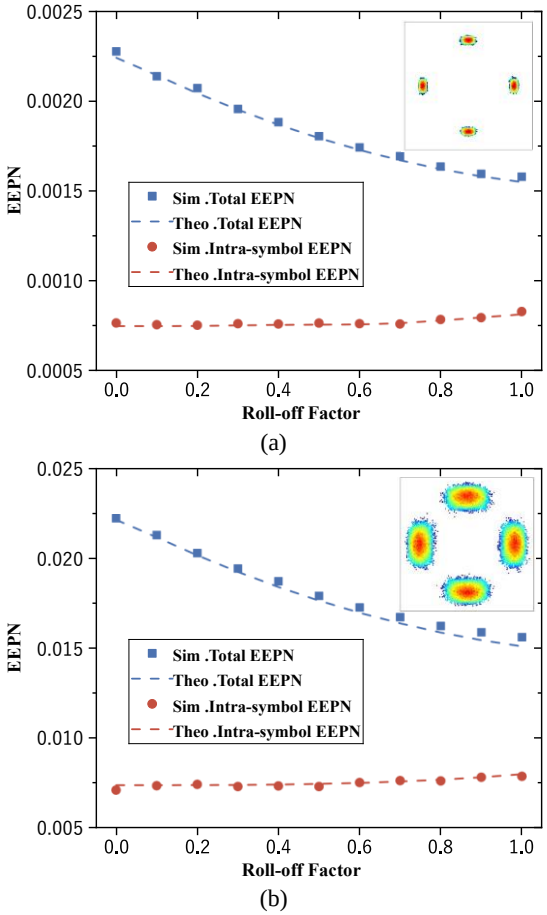

Fig. 4. Intra-symbol and total EEPN for different roll-off factors when transmitting QPSK signals. The laser linewidths for (a) and (b) are 100 kHz and 1 MHz, respectively. The insets display degraded QPSK signal constellations with $\beta = 1$.

III. Modulus-dependent EEPN for High-Order Modulation Formats

In [15], Lau *et al*. showed that EEPN-induce phase noise is twice that of the EEPN-induce amplitude noise for QPSK signals by simulation. Subsequently, we defined the concept of ovality for constellation clusters and extended this definition to higher-order modulation formats with multiple moduli in [13]. The modulus-dependent EEPN distributions of the oval constellation clusters have been explained and calculated by noting that intra-symbol EEPN scales with the power of individual constellation cluster, whereas inter-symbol EEPN scales with the average power of the whole constellation.

In this section, we update our results in [13] by including the results in Section II. Similarly, denote a set of constellation points/clusters as C, and the i^{th} constellation point as C_i. For each constellation cluster with different modulus, the total EEPN is

$$EEPN[C_i] = |C_i|^2 \cdot EEPN_{\text{intra}} + E[|C|^2] \cdot EEPN_{\text{inter}} \quad (15)$$

where $|C_i|^2$ represents the power of the i^{th} constellation point. In Eq. (15), the average power of the whole constellation is normalized to unity. The two terms in Eq. (15) represent the intra-symbol and inter-symbol EEPN of the individual constellation points. It is evident that constellation points with the same modulus have the same EEPN.

According to our study in [13], we can express the constellation clusters in the polar coordinates $C_i = re^{j\varphi}$, and the total EEPN can be divided into EEPN-induce phase and amplitude noise. The intra-symbol EEPN ($|C_i|^2 \cdot EEPN_{\text{intra}}$) only includes phase noise, and the inter-symbol EEPN ($E[|C|^2] \cdot EEPN_{\text{inter}}$) is equally split to the phase and amplitude noise [13][15]. Therefore, the scaled phase noise and amplitude noise of EEPN for high-order modulation are given as

$$EEPN[r\varphi, C_i] = \frac{1}{2} E[|C|^2] \cdot EEPN_{\text{inter}} + |C_i|^2 \cdot EEPN_{\text{intra}} \quad (16)$$

$$EEPN[r, C_i] = \frac{1}{2} E[|C|^2] \cdot EEPN_{\text{inter}}. \quad (17)$$

Then the ratio of EEPN-induced phase and amplitude noise is the ovality, showing the degree to which the constellation clusters deviate from a circular distribution [13], given by

$$O(C_i) = \frac{EEPN[r\varphi, C_i]}{EEPN[r, C_i]} = \frac{\frac{1}{2} E[|C|^2] \cdot EEPN_{\text{inter}} + |C_i|^2 \cdot EEPN_{\text{intra}}}{\frac{1}{2} E[|C|^2] \cdot EEPN_{\text{inter}}}. \quad (18)$$

We conducted a simulation of 16QAM transmission to illustrate the variation in ovality, and the results are depicted in Fig. 5. From the constellations, the outer ring consistently exhibits greater ovality compared to the inner ring. Additionally, the overall noise spreading of the constellations with a roll-off factor of 1 is smaller compared to those with a roll-off factor of 0. This again shows that higher roll-off factors induce lower EEPN. Fig. 5 (c) demonstrates that ovality increases with the roll-off factor, with the outer ring showing a much more significant increase. Notably, the simulation results closely match the theoretical predictions. In addition, the overall noise is apparently larger in the outer ring clusters with a larger modulus.

Table I lists the calculated values of ovality for several QAM constellations with roll-off factor of 0 and 1, respectively. Again, the outer rings and larger roll-off factor both lead to larger ovality. For example, the ovality of the outer ring of 32QAM can significantly increase from 2.71 to 4.78.

TABLE 1 Ovality for different QAMs
(Ovality for $\beta = 1$ is updated within brackets)

$\lvert C_i \rvert^2$	2	10	18	26	34
8QAM	1.33(1.74)	2.67(4.71)			
16QAM	1.20(1.44)	2.00(3.22)	2.80(5.00)		
32QAM	1.10(1.22)	1.50(2.11)	1.91(3.00)	2.31(3.89)	2.71(4.78)

Finally, we have assumed perfect LO phase noise compensation. If we consider practical carrier phase recovery, the overall EEPN can be reduced to the inter-symbol EEPN only, as demonstrated in [13], because the phase compensation squeezes the phase noise. Fig. 6 illustrates the reduced total EEPN for QPSK and 16QAM by blind phase searching (BPS). The simulation results corroborate the analytical expressions. The reduction is more significant at higher roll-off factors, attributed to increased ovality or stronger phase noise. Note that the results for QPSK and 16QAM are nearly overlapped, because our analysis of total EEPN does not incorporate any modulation format-specific parameters, making the results independent of the modulation formats.

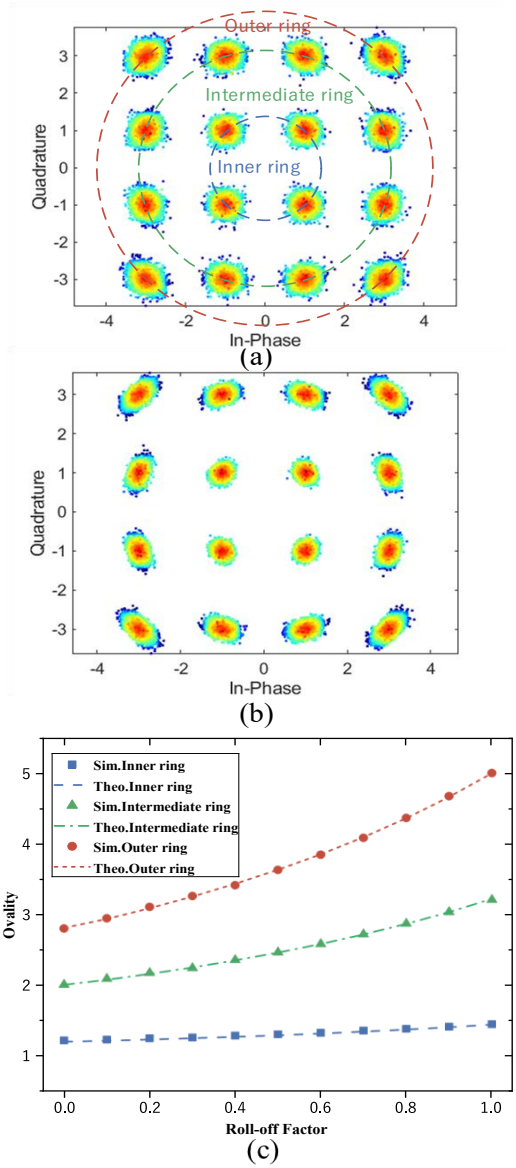

Fig. 5. Ovality for different roll-off factors: (a) 0 and (b) 1 for 16QAM with a 100 kHz laser linewidth. (c) Ovality versus roll-off factor for the three rings of 16QAM constellation.

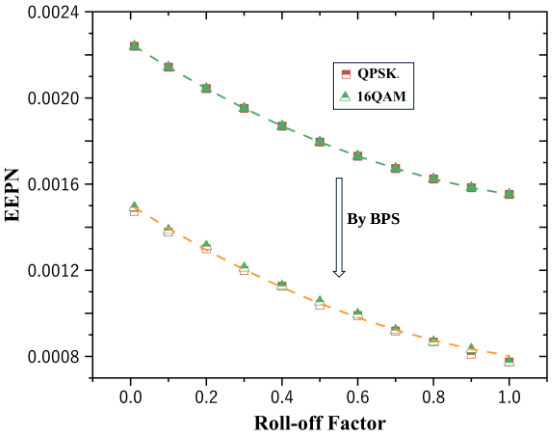

Fig. 6. Reduced total EEPN by BPS versus roll-off factor for QPSK and 16QAM, respectively. Their EEPN results for are nearly overlapped. The dashed lines represent the analytical expressions.

IV. Conclusion

In this paper, we have conducted a detailed analysis of EEPN for coherent optical transceivers with arbitrary roll-off factors. We have elucidated that the transmission channel affected by EEPN is non-unitary when the roll-off factor is non-zero. By calculating the resulting energy loss, we have updated the closed-form expressions for intra-symbol, inter-symbol, and total EEPN. Our theoretical calculations and simulations have shown that total and inter-symbol EEPN decrease with larger roll-off factors, while intra-symbol EEPN remains approximately constant. Furthermore, we have extended our analysis to higher order modulation formats with modulus-dependent EEPN distributions, revealing that ovality also increases with the roll-off factor..

Appendix
Derivation of Generalized EEPN

In this appendix, we provide the detailed derivations. First, the frequency response of RC filter is given as

$$H_{rc}=\begin{cases}T_s, 0\le|f|\le\dfrac{1-\beta}{2T_s}\\ \dfrac{T_s}{2}\left\{1+\cos\left[\dfrac{\pi\left(|f|-\dfrac{1-\beta}{2T_s}\right)T_s}{\beta}\right]\right\}, \dfrac{1-\beta}{2T_s}\le|f|\le\dfrac{1+\beta}{2T_s}\\ 0, \text{otherwise}\end{cases}. \quad (A1)$$

whose time response is

$$h_{rc}(t)=\frac{\sin\left(\dfrac{\pi t}{T_s}\right)}{\dfrac{\pi t}{T_s}}\cdot\frac{\cos\left(\dfrac{\beta\pi t}{T_s}\right)}{1-\left(\dfrac{2\beta t}{T_s}\right)^2}. \quad (A2)$$

The spectral density $S(f)$ of the Wiener phase noise

follows a Lorentzian line shape, given as

$$S(f)=\frac{1}{2\pi}\frac{f_{3dB}}{f^2+\left(\frac{f_{3dB}}{2}\right)^2}, \tag{A3}$$

where f_{3dB} is the 3dB-linewidth of the LO laser.

The frequency response due to fiber dispersion is

$$H_f(f)=e^{jrf^2}, \tag{A4}$$

where $r=2\pi^2|\beta_2|l$ is the dispersion related parameter, β_2 is the group vector dispersion (GVD), and l is the length of optic fiber. The electrical dispersion equalizer's response is the conjugate of that of fiber dispersion.

Then, substituting Eq. (A2) (A3) into Eq. (9), we arrive at

$$E_{1,\text{total}}=\frac{1}{2\pi^2}\sum_{n=-\infty}^{\infty}\int_{-\infty}^{\infty}\frac{\sin^2(rf/T_s)}{(n\pi+rf/T_s)^2}\cdot\frac{\cos^2\left(n\beta\pi+\frac{\beta rf_{3dB}/T_s}{2}\right)}{\left(1-\left(2n\beta+\frac{2\beta rf/T_s}{\pi}\right)^2\right)^2}\cdot\frac{f_{3dB}}{f^2+\left(\frac{f_{3dB}}{2}\right)^2}df \tag{A5}$$

By following a similar calculation in [6], we can calculate the exact result of Eq. (A5) as

$$E_{1,\text{total}}=\frac{4-\beta}{4}+\frac{\beta}{4}e^{-2\alpha}. \tag{A6}$$

which can be approximately as

$$E_{1,\text{total}}\approx 1-\frac{\beta}{2}\alpha. \tag{A7}$$

Another important calculation is for the average energy of the received signal. Following the discussion in [6], we first calculate the average of the isolated "1" symbol after transmission, given by

$$E[y_1(t)]=\int_{-\infty}^{\infty}h_{rc}(t)\otimes h_f(t-\tau)E[e^{j(\phi_r(t-\tau)-\phi_r(0))}]h_e(\tau)d\tau \tag{A8}$$

.

We convert it to the frequency domain as

$$\begin{aligned}&E[y_1(t)]\\&=\int_{-\infty}^{\infty}h_{rc}(t)\otimes h_f(t-\tau)\cdot\int_{-\infty}^{\infty}S(f)e^{j2\pi f(t-\tau)}df\cdot h_e(\tau)d\tau\\&=\int_{-\infty}^{\infty}S(f)\int_{-\infty}^{\infty}H_{rc}(f)H_f(f_1-f)H_e(f)e^{j2\pi ft}df_1df\end{aligned} \tag{A9}$$

Similar to Eq. (A8), we calculate the second order moment as

$$E[|y_1(t)|^2]=\int_{-\infty}^{\infty}S(f)\left|\int_{-\infty}^{\infty}H_{rc}(f)H_f(f_1-f)H_e(f)e^{j2\pi ft}df_1\right|^2df, \tag{A10}$$

We need to evaluate them at the corectly sampled point, t=0. Subsequently, we calculate their respective exact results as

$$\begin{aligned}E[y_1(0)]&=\frac{1}{2\alpha}(2-e^{-(1+\beta)\alpha}-e^{-(1-\beta)\alpha})\\&+\frac{2\alpha\beta^2}{\pi^2+4\beta^2\alpha^2}\cdot[e^{-(1+\beta)\alpha}+e^{-(1-\beta)\alpha}\\&-\cos(\frac{1+\beta}{2\beta}\pi)-\cos(\frac{1-\beta}{2\beta}\pi)]\end{aligned} \tag{A11}$$

$$\begin{aligned}&E[|y_1(0)|^2]\\&=\frac{1}{4\alpha^2}[-1+e^{-2\alpha}-e^{-2\beta\alpha}+\frac{1}{2}e^{-2(1+\beta)\alpha}+\frac{1}{2}e^{-2(1-\beta)\alpha}]\\&+\frac{1}{2\alpha}(2-\beta)\\&+\frac{\beta^2}{\pi^2+4\beta^2\alpha^2}[-e^{-2(1-\beta)\alpha}-e^{-2(1+\beta)\alpha}-2e^{-2\alpha}+2e^{-2\beta\alpha}\\&+2+\alpha\beta+\frac{\alpha}{2}(1-\beta)\cos(\frac{1-\beta}{\beta}\pi)\\&+\frac{\alpha}{2}(1+\beta)\cos(\frac{1+\beta}{\beta}\pi)+\frac{\alpha}{2}\cos(\frac{\pi}{\beta})\\&-\frac{2}{\pi}\beta\alpha\sin(\frac{1+\beta}{\beta}\pi)\\&-\frac{2}{\pi}\beta\alpha\sin(\frac{1-\beta}{\beta}\pi)-\frac{4}{\pi}\beta\alpha\sin(\frac{1}{\beta}\pi)]\\&+(\frac{2\alpha\beta^2}{\pi^2+4\beta^2\alpha^2})^2\\&\cdot[-1+e^{-2\alpha}-e^{-2\beta\alpha}+\frac{1}{2}e^{-2(1+\beta)\alpha}+\frac{1}{2}e^{-2(1-\beta)\alpha}]\end{aligned} \tag{A12}$$

Finally, the inter-symbol EEPN can be given as

$$EEPN_{\text{intra}}=D[y_1(0)]==E[|y_1(0)|^2]-|E[y_1(0)]|^2 \tag{A13}$$

REFERENCES

[1] X. Chen *et al.*, "All-Electronic 100-GHz Bandwidth Digital-to-Analog Converter Generating PAM Signals up to 190 GBaud," *J. Light. Technol.*, vol. 35, no. 3, pp. 411-417, 1 Feb.1, 2017.

[2] Xi Chen, Prashanta Kharel, Greg Raybon, Di Che, Christian Reimer, Kevin Luke, Mian Zhang, "Demonstration of 120-GBaud 16-QAM Driver-less Coherent Transmitter with 80-km SSMF Transmission", 2022 Optical Fiber Communications Conference and Exhibition (OFC), pp.1-3, 2022.

[3] X. Zhou, R. Urata, and H. Liu, "Beyond 1Tb/s Datacenter Interconnect Technology: Challenges and Solutions (Invited)," in *Optical Fiber Communication Conference (OFC) 2019*, OSA Technical Digest (Optica Publishing Group, 2019), paper Tu2F.5.

[4] E. Maniloff, S. Gareau and M. Moyer, "400G and Beyond: Coherent Evolution to High-Capacity Inter Data Center Links," *2019 Optical Fiber Communications Conference and Exhibition (OFC)*, San Diego, CA, USA, 2019, pp. 1-3.

[5] H. Xu, M. O. Rebellato, and S. Wang, "System Impact of Laser Phase Noise On 400G and Beyond Coherent Pluggables," in *Optical Fiber Communication Conference (OFC) 2023*, Technical Digest Series (Optica Publishing Group, 2023), paper Th1E.1.

[6] W. Shieh and K.-P. Ho, "Equalization-enhanced phase noise for coherent detection systems using electronic digital signal processing," *Opt. Exp.*, vol. 16, no. 20, pp. 15718–15727, Sep. 2008.

[7] A. Kakkar, J. R. Navarro, R. Schatz, H. Louchet, X. Pang, O. Ozolins, G. Jacobsen, and S. Popov, "Comprehensive Study of Equalization-Enhanced Phase Noise in Coherent Optical Systems," *J. Light. Technol.*, vol. 33, no. 23, pp. 4834–4841, Dec. 2015.

[8] A. Arnould and A. Ghazisaeidi, "Equalization Enhanced Phase Noise in Coherent Receivers: DSP-Aware Analysis and Shaped Constellations," *J. Light. Technol.*, vol. 37, no. 20, pp. 5282–5290, Oct. 2019.
[9] G. Colavolpe, T. Foggi, E. Forestieri, and M. Secondini, "Impact of Phase Noise and Compensation Techniques in Coherent Optical Systems," *J. Light. Technol.*, vol. 29, no. 18, pp. 2790–2800, Sep. 2011, doi: 10.1109/JLT.2011.2164237.
[10] K.-P. Ho, A. Pak Tao Lau, and W. Shieh, "Equalization-enhanced phase noise induced timing jitter," *Opt. Lett.*, vol. 36, no. 4, pp. 585, Feb. 2011.
[11] C. Jin, N. A. Shevchenko, Z. Li, S. Popov, Y. Chen, and T. Xu, "Nonlinear Coherent Optical Systems in the Presence of Equalization Enhanced Phase Noise," *J. Light. Technol.*, vol. 39, pp. 4646-4653, Jun. 2021.
[12] K. P. Ho and W. Shieh, "Equalization-enhanced phase noise in mode-division multiplexed systems," *J. Light. Technol.*, vol. 31, no. 13, pp. 2237–2243, Jul. 2013.
[13] H. Wang, X. Yi, J. Zhang and F. Li, "Extended Study on Equalization-Enhanced Phase Noise for High-Order Modulation Formats," *J. Lightw. Technol.*, vol. 40, no. 24, pp. 7808-7813, 15 Dec.15, 2022.
[14] X. Yi, H. Wang and J. Zhang, "Reducing Equalization-enhanced Phase Noise via Carrier Phase Recovery in the Presence of Variable Matched-filter Bandwidth," *2023 Photonics & Electromagnetics Research Symposium (PIERS)*, Prague, Czech Republic, 2023, pp. 1887-1891.
[15] A. P. T. Lau, T. S. R. Shen, W. Shieh, and K.-P. Ho, "Equalization-enhanced phase noise for 100Gb/s transmission and beyond with coherent detection," *Opt. Exp.*, vol. 18, no. 16, pp. 17239–17251, Aug. 2010.